Statistical Analysis and Model Validation of a UWB Innovative Phased Array for M-AESA Applications

Andrea Petricca, Christian Canestri, Cosmo Mitrano, Riccardo Ardoino, Walter Fuscaldo, and Alessandro Galli

Abstract – This paper presents a novel analysis, design, and test of an ultra-wideband (UWB) phased array for Multifunctional Active Electronically Scanned Array (M-AESA) applications. The 2-D array is designed to work from 1 GHz to 6 GHz (i.e., from L to C band), providing more than two octaves of frequency band. The radiating element is the so-called connected Vivaldi antenna, which exploits here the "connected array" concept. It provides low cost and a simplified integration, with good matching properties, good polarization purity, excellent realized gain, and very high total efficiency. An innovative rigorous statistical analysis has been developed, which accounts for the quantization and uncertainty of complex excitations in terms of both amplitude and phase coefficients. Finally, an experimental validation has also been performed on a proof-of-concept connected Vivaldi array prototype. The excellent agreement between measurements and simulations looks really promising.

1. Introduction

During the past decades, phased array antennas were widely used in several applications, such as control systems, telecommunications, remote sensing, and radiometry [1]. The combination of phased array architectures with multifunctional radio frequency (RF) systems has given rise to the so-called multifunctional active electronically scanned arrays (M-AESAs) [2]. M-AESA architectures allow to serve for radar, communications, and electronic support applications. A radiating element used for this kind of applications is the Vivaldi antenna. The standard microstrip Vivaldi antenna [3, 4] typically suffers from impedance matching issues, relatively high levels of cross-polarization, and lattice resonances. Good performances have been obtained by designing ad hoc structures to reduce mutual coupling effects [5, 6] or by exploiting a PCB feeding section and a metallic antenna design [7]. Moreover, it has been shown that "slicing" the Vivaldi metallic flares significantly improves the polarization purity [8].

In this frame, good performance has been achieved by using an innovative connected Vivaldi antenna [9], which is based on the *connected array approach* [10–14]. In particular, all radiating elements of the array are electrically connected, enhancing the mutual coupling between them, to realize a bulk array structure that allows for improving the realized gain, total efficiency, polarization purity, and matching properties. A connected version of the Vivaldi antenna, although different from the one presented here, has very recently appeared within the framework of the Square Kilometre Array (SKA) project [15, 16].

An innovative rigorous statistical analysis has also been performed here to test the robustness of the entire architecture. The most common errors on phased array complex excitations (amplitude and phase) are related to *quantization* and *fabrication* (random errors) issues. Quantization errors arise from the use of phase shifters with a finite number of bits and of power distribution networks that provide a finite number of amplitude states, whereas the random errors are due to various fabrication tolerances on the monolithic microwave integrated circuits (MMICs). Experimental tests have finally been performed on a proof-of-concept prototype of the Vivaldi array.

The outline of the work is as follows. In Section 2 the simulation results for the array analysis and design are shown, and in Section 3 the results of the statistical analysis on the designed array factor are discussed. In Section 4 the experimental validation on the demonstrator prototype is illustrated, and conclusions are drawn in Section 5.

2. Antenna Array Design

The proposed array is designed to work in the frequency band from 1 GHz to 6 GHz. It consists of 24 elements arranged in a planar lattice with four rows and six columns. In this paper, the "Ludwig II Azimuth over Elevation" coordinate system [17] is used, where the z-axis represents the boresight direction (direction orthogonal to the plane of the array). The principal planes are the azimuth (xz) plane and the elevation (yz) plane. The simulation model of the designed array is shown in the inset of Figure 1. A triangular grid lattice has been selected [18, ch. 2], since it allows the effective interelement distance on the azimuth plane to

Manuscript received 28 August 2020.

Andrea Petricca and Alessandro Galli are with the Department of Information Engineering, Electronics and Telecommunications, Sapienza University of Rome, Via Eudossiana 18, 00184 Rome, Italy; e-mail: petricca.1637715@studenti.uniroma1.it, alessandro.galli@uniroma1.it.

Christian Canestri, Cosmo Mitrano, and Riccardo Ardoino are with Elettronica S.p.A., 00131 Via Tiburtina Valeria 13700, Rome, Italy; e-mail: christian.canestri@elt.it, cosmo.mitrano@elt.it, riccardo.ardoino@elt.it.

Walter Fuscaldo is with the Consiglio Nazionale delle Ricerche, Istituto per la Microelettronica e Microsistemi (CNR-IMM), 00133 Via del Fosso del Cavaliere 100, Rome, Italy; e-mail: walter.fuscaldo@cnr.it.

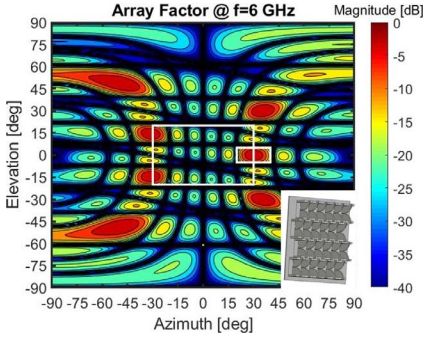

Figure 1. Contour plot of the array factor at 6 GHz for the critical scanning case on the azimuth plane. In the inset a view of the array is shown.

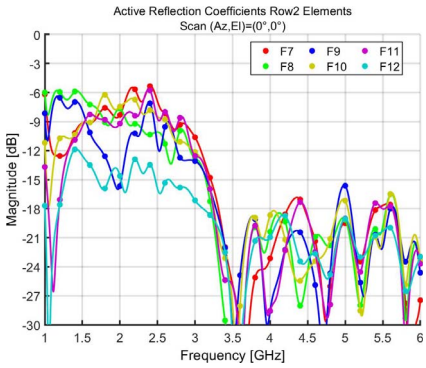

Figure 2. F-parameters of the radiating elements in the second row for boresight pointing.

be reduced with respect to the standard rectangular grid, thus promoting optimal separation of the first grating lobes. The array factor for the critical scanning angle on the azimuth plane ($\mathrm{Az} = 30^{\circ}$, $\mathrm{El} = 0^{\circ}$) at the maximum frequency within the operating band (6 GHz) is sketched in Figure 1. The main lobe is bounded with a white rectangle. The other greater white rectangle bounds the interested visible region, in this work $-30° < \mathrm{Az} < 30°$ and $-15° < \mathrm{El} < 15°$.

The designed connected Vivaldi is a completely metallic structure that exploits a simplified feeding section, an exponential profile (typical of Vivaldi antennas), and two metallic septa to avoid undesired lattice resonances. The radiating element ensures very high levels of total efficiency (above 70%, meant as average among the array elements and within the operating frequency band). The antenna array has been designed using the full-wave commercial software CST Microwave Studio [19]. The average element pattern takes into account the behavior of each element displaced in different positions on the array lattice, and it has been computed via postprocessing in MATLAB [20].

In Figure 2 the active reflection coefficients (or F-parameters) of the elements in the second row are reported for the boresight pointing case.

It should be noted that the single F-parameter represents the reflection coefficient when the other ports are excited. The maximum amplitude of the F-parameters is about –6 dB, which represents a rather acceptable level. The average boresight realized gain versus frequency is reported in Figure 3, where the average total efficiency is also represented for both the designed connected Vivaldi array and a standard microstrip Vivaldi array considering the same lattice geometry.

The cross-polar component is at least 18 dB lower than the main polarization across the bandwidth, considering the boresight direction, whereas the trend of the average element pattern is rather regular with proper half-power beamwidths (HPBWs), as can be inferred from the plot on the principal planes reported in Figure 4 at 1 GHz, 3 GHz, and 6 GHz.

3. Statistical Analysis Results

For a more accurate evaluation of the achievable performance of the proposed array topology, a rigorous statistical analysis has been performed considering quantization and uncertainty errors on the complex excitation coefficients.

Quantization errors on array element excitations were studied in [18, ch. 6]. A mathematical model has been implemented here on MATLAB to characterize quantization errors on the designed array factor. The general expression of the array factor has the following form:

$$\mathrm{AF}(\hat{\mathbf{r}}) = \sum_{n=1}^{N} A_n e^{j\alpha_n} e^{jk\hat{\mathbf{r}}\cdot\mathbf{r}_n} \tag{1}$$

where $\hat{\mathbf{r}} \equiv (\mathrm{Az}, \mathrm{El})$ is the observation point unit vector, N is the number of array elements, $\mathbf{r}_n$ is the position of the nth element, A_n and α_n are its excitation amplitude and phase, respectively, and k is the free-space wavenumber. The excitation phases are chosen to scan the main lobe at $\hat{\mathbf{r}}_0$: $\alpha_n = -k\hat{\mathbf{r}}_0 \cdot \mathbf{r}_n$.

The excitation amplitude of the nth element is quantized as follows:

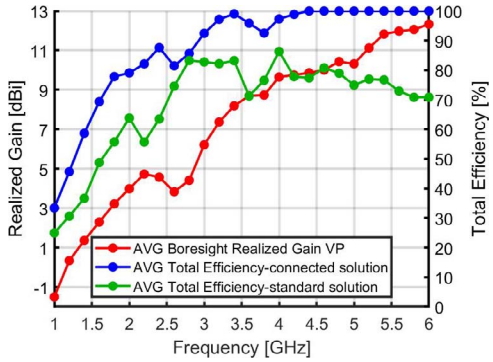

Figure 3. Average element boresight realized gain and total efficiency for connected and standard arrays.

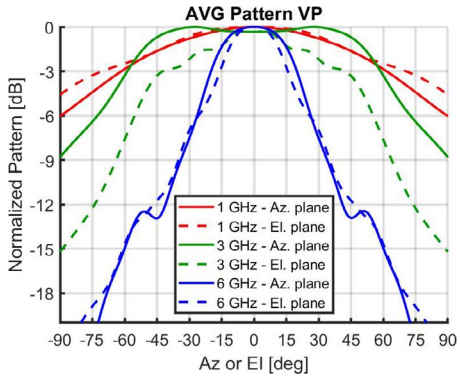

Figure 4. Normalized average element pattern on the principal planes.

$$\overline{A'_n} = Q\left[\frac{A_n}{\max\limits_m(A_m)}\right] \tag{2}$$

where A_n and $\overline{A'_n}$ are the excitation amplitudes of the ideal (nonquantized) and nonideal case, respectively (the latter being normalized to its maximum), whereas the function Q[·] indicates the quantized ratio between the ideal excitation amplitude of the current element and the maximum ideal excitation amplitude. When expressed in decibels, the function $Q(x)$ can assume only the following quantized values:

$$\mathrm{Q}(x)\ (\mathrm{dB}) \in \{-d, \ldots, -2d/(N_\mathrm{s}-1), -d/(N_\mathrm{s}-1), 0\} \tag{3}$$

where $d \in \mathbb{R}^+$ and $N_s \in \mathbb{N}$ indicate the dynamic range and the number of states, respectively, of the quantization process. The quantization step s is given by $s = d/(N_\mathrm{s}-1)$. In real applications, usual values are $d = 20$ dB and $s = 2.5$ dB.

The phase excitation of the nth element (α'_n) is quantized considering the corresponding ideal case excitation phase (α_n) and taking the closest quantization level. The quantization levels are then given by

$$(p-1)\frac{2\pi}{2^{N_\mathrm{b}}} \quad p = 1, \ldots, 2^{N_b} \tag{4}$$

where N_b is the number of bits for each phase shifter.

To have a basic idea of the influence of such nonideality in the array performance, we discuss here just a numerical example considering four-bit phase shifters and a uniform excitation, thus neglecting the amplitude quantization. Table 1 represents the absolute value of the error between the ideal and the quantized excitation phases when the main lobe scan is at $(\mathrm{Az}, \mathrm{El}) = (20^\circ, 0^\circ)$.

The periodic nature of the phase error causes relatively high sidelobes, known in the literature as *quantization lobes* [18, ch. 6]. This effect is manifest in Figure 5, where the array factor of the quantized case (green line) is compared with that of the ideal case (red line) at 6 GHz.

Table 1. Color map of the phase error (in degrees) for the 24 elements of the array.

Phase Error [deg]

Row index \ Column index	1	2	3	4	5	6
1	0,00	10,63	1,25	9,38	2,49	8,14
2	5,94	4,69	7,18	3,45	8,43	2,20
3	0,00	10,63	1,25	9,38	2,49	8,14
4	5,94	4,69	7,18	3,45	8,43	2,20

Quantization lobes are present in the nonideal case, e.g., at $\mathrm{Az} \simeq -45^\circ$. We note that their amplitudes do not follow the quasimonotonically decreasing trend that can be observed for the ideal case.

With regard to random errors, a mathematical model has also been implemented on MATLAB to study their effect ([1, 18, ch. 6]) on the excitations for the designed array. In the nonideal case (i.e., with uncertainty), the excitation amplitude of the nth element is computed from the ideal case as in the following equation:

$$A'_n = A_n(1+\delta_n) \quad n = 1, \ldots, N \tag{5}$$

where δ_n $(n = 1, \ldots, N)$ are independent and identically distributed (i.i.d.) random variables with zero mean and uniform distribution. Although a Gaussian distribution is a more conventional choice, the uniform distribution is chosen here as it allows for evaluating the array performance in the worst-case scenario.

In fact, a uniform distribution features a higher standard deviation with respect to a Gaussian distribution under the same peak-to-peak variation. Similarly, the nonideal phase of the nth element is computed as in the following equation:

$$\alpha'_n = \alpha_n + \varphi_n \quad n = 1, \ldots, N \tag{6}$$

where φ_n $(n = 1, \ldots, N)$ are i.i.d. random phase errors with zero mean and uniform distribution.

An example of MATLAB simulation is considered, where the main lobe is scanned at $(\mathrm{Az}, \mathrm{El}) = (20^\circ, 0^\circ)$, and the peak-to-peak amplitude and phase errors are 1 and 30°, respectively. For the nonideal case excitations, 1000 realizations have been generated, over which the squared amplitude of the array factor has been averaged. Simulation results are presented in Figure 5, where the ideal (red line) and the average nonideal case (blue line) array factors are compared at 6 GHz. As described in [1, 18, ch. 6], the residual effect on the nonideal case array factor is evident. This effect cancels the array factor nulls and it is referred to as *residual sidelobe level*. Other typical effects due to random excitation uncertainty, although less evident in Figure 5, are beam-pointing errors and directivity reductions. In Figure 5, several single

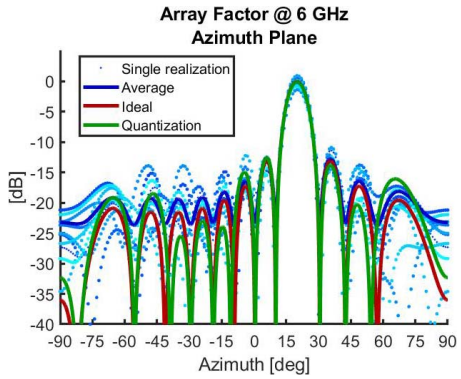

Figure 5. Effects of quantization and uncertainty errors on the designed array factor.

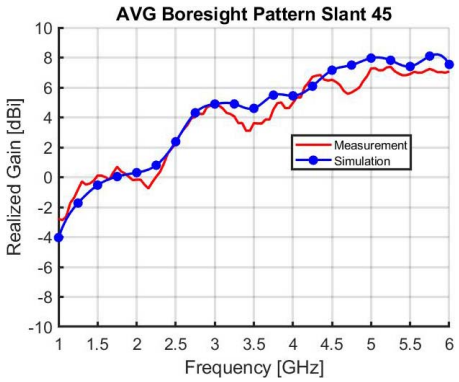

Figure 7. Boresight gain comparison between measurements and simulations.

realizations also are reported for the nonideal case. They almost overlap at the pointing direction and gradually spread around the ideal case array factor nulls.

4. Experimental Validation

An experimental validation of the proposed design has also been performed on a connected Vivaldi array prototype manufactured at Elettronica SpA. Although this first prototype is not strictly equivalent to the layout described in Section 2, the experimental validation here reported is fundamental as a proof of concept of the overall presented study. The manufactured prototype consists of an array composed by eight connected Vivaldi elements (see the inset of Figure 6) that work between 1 GHz and 6 GHz. The measurement results have been evaluated within the StarLab near field facility [21].

In Figure 6, the reflection coefficient of a central element is reported, and the average element boresight realized gain is shown in Figure 7.

The excellent agreement between measurements and simulations not only fully validates the innovative radiating element technology, but also looks very promising for the validation of other topologies of such arrays based on connected Vivaldi antennas in various M-AESA applications.

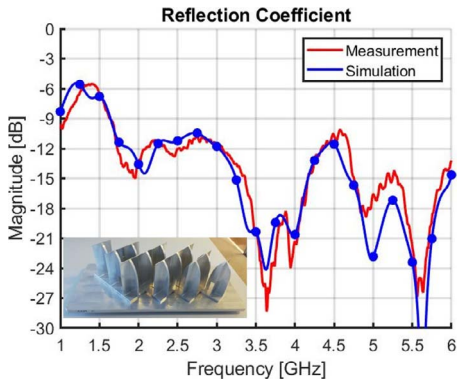

Figure 6. Reflection coefficient comparison between measurements and simulations.

5. Conclusions

In this paper the design, optimization, and test of a UWB phased array for M-AESA applications have been described. The use of an innovative radiating element, the connected Vivaldi, has played a key role in obtaining extremely good performance, especially in terms of matching, boresight realized gain, and total efficiency over a large bandwidth.

For a better characterization of the array performance, a novel statistical analysis of the quantization of excitations and uncertainty effects has been carried out with an ad hoc mathematical model, thus providing a powerful tool to analyze the array performance taking into account nonideality effects.

The experimental validation performed on a proof-of-concept prototype of a connected Vivaldi array has confirmed the reliability of this innovative radiating element technology. The present work may therefore pave the way for the development of UWB high-performance arrays based on modularity concepts and cost-effective solutions.

6. References

1. D. Parker and D. C. Zimmermann, “Phased Arrays–Part I: Theory and Architectures,” *IEEE Transactions on Microwave Theory and Techniques*, **50**, 3, March 2002, pp. 678–687.
2. S. Kemkemian and M. Nouvel-Fiani, “Toward Common Radar & EW Multifunction Active Arrays,” IEEE International Symposium on Phased Array Systems and Technology, Waltham, MA, USA, October 12–15, 2010.
3. P. J. Gibson, “The Vivaldi Aerial,” 9th European Microwave Conference, Brighton, UK, September 17–20, 1979, doi: 10.1109/EUMA.1979.332681.
4. J. Shin and D. H. Schaubert, “A Parameter Study of Stripline-Fed Vivaldi Notch-Antenna Arrays,” *IEEE Transactions on Antennas and Propagation*, **47**, 5, May 1999, pp. 879–886.
5. S. Zhu, H. Liu, P. Wen, Z. Chen, and H. Xu, “Vivaldi Antenna Array Using Defected Ground Structure for Edge Effect Restraint and Back Radiation Suppression,” *IEEE*

Antennas and Wireless Propagation Letters, **19**, 1, January 2020, pp. 84–88.
6. B. Wu, H. Wang, X. Liu, Z. Ding, S. Quan, J. Cao, and P. Soothar, "Optimization to the Scan Blindness of Vivaldi Array With Metallic T-Shaped Structure," 2019 IEEE MTT-S International Wireless Symposium (IWS), Guangzhou, China, May 19–22, 2019.
7. H. Kähkönen, J. Ala-Laurinaho, and V. Viikari, "Dual-Polarized Ka-Band Vivaldi Antenna Array," *IEEE Transactions on Antennas and Propagation*, **68**, 4, April 2020, pp. 2675–2683.
8. R. W. Kindt and J. T. Logan, "Dual-Polarized Metal-Flare Sliced Notch Antenna Array," *IEEE Transactions on Antennas and Propagation*, **68**, 4, April 2020, pp. 2666–2674.
9. C. Canestri, D. Gaetano, P. Bia, A. Manna, and C. Mitrano, "An Innovative UWB Connected Array for Multifunctional Applications," 2019 IEEE International Symposium on Antennas and Propagation and USNC-URSI Radio Science Meeting, Atlanta, GA, USA, July 7–12 2019.
10. R. C. Hansen, "Non-Foster and Connected Planar Arrays," *Radio Science*, **39**, 2004, p. RS4004.
11. R. C. Hansen, "Linear Connected Arrays," *IEEE Antennas and Wireless Propagation Letters*, **3**, 2004, pp. 154–156.
12. H. Wheeler, "Simple Relations Derived From a Phased Array Antenna Made of an Infinite Current Sheet," *IEEE Transactions on Antennas and Propagation*, **13**, 4, July 1965, pp. 506–514.
13. A. Neto, D. Cavallo, G. Gerini, and G. Toso, "Scanning Performances of Wideband Connected Arrays in the Presence of a Backing Reflector," *IEEE Transactions on Antennas and Propagation*, **57**, 10, October 2009, pp. 3092–3102.
14. D. Cavallo, A. Neto, G. Gerini, and F. Smiths, "Connected Arrays of Dipoles for Broad Band, Wide Angle Scanning, Dual Polarized Applications: A Novel Solution to the Common Mode Problem," 2010 International Symposium on Phased Array Systems and Technology, Waltham, MA, USA, October 12–15, 2010.
15. M. Ruiter, W. van Cappellen, E. van der Wal, M. Arts, R. van den Brink, et al., "Development of a Vivaldi Tile for the SKA Mid Frequency Aperture Array," 10th European Conference on Antennas and Propagation (EuCAP), Davos, Switzerland, April 10–15, 2016.
16. R. Z. Syeda, J. G. bij de Vaate, and D. Prinsloo, "Regular and Irregular-on-Grid Sparse Array Comparison of Connected Aperture Arrays," *IEEE Antennas and Wireless Propagation Letters*, **19**, 4, April 2020, pp. 586-590.
17. G. Masters and S. Gregson, "Coordinate System Plotting for Antenna Measurements," AMTA Annual Meeting and Symposium, St. Louis, MO, USA, 2007, pp. 1–10.
18. R. J. Mailloux, *Phased Array Antenna Handbook*, 2nd ed., Norwood, MA, Artech House, 2005.
19. CST - Computer Simulation Technology, *CST Microwave Studio*, version 2019, Darmstadt, Germany, CST - Computer Simulation Technology AG.
20. MathWorks, *MATLAB*, version R2013a. Natick MA, USA, MathWorks.
21. L. Duchesne, P. Garreau, N. Robic, A. Gandois, P. O. Iversen, et al., "Compact Multi-Probe Antenna Test Station for Rapid Testing of Antennas and Wireless Terminals," AMTA, Atlanta, GA, USA, October 2004.